Article

Microrheology with Fluorescence Correlation Spectroscopy

Silke Rathgeber, Hans-Josef Beauvisage, Hubert Chevreau, Norbert Willenbacher, and Claude Oelschlaeger

Langmuir, **Article ASAP** • Publication Date (Web): 08 May 2009

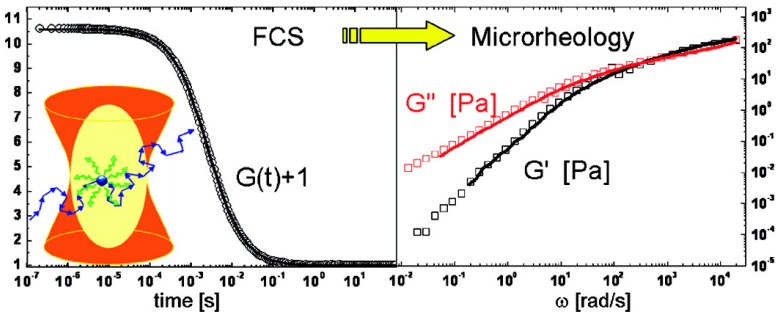

More About This Article

Additional resources and features associated with this article are available within the HTML version:

- Supporting Information
- Access to high resolution figures
- Links to articles and content related to this article
- Copyright permission to reproduce figures and/or text from this article

View the Full Text HTML

Langmuir
Article
pubs.acs.org/Langmuir

Microrheology with Fluorescence Correlation Spectroscopy

Silke Rathgeber,*[,†,‡] Hans-Josef Beauvisage,[†] Hubert Chevreau,[†,§] Norbert Willenbacher,[∥] and Claude Oelschlaeger[∥]

[†]*Max Planck-Institute for Polymer Research, Polymer Physics, 55128 Mainz, Germany,* [‡]*Johannes Gutenberg-University Mainz, Institute for Physics, 55099 Mainz, Germany,* [§]*Ecole Polytechnique Universitaire de Lille, 59655 Villeuneuve D'Ascq Cedex, France, and* [∥]*Technical University Karlsruhe, 76131 Karlsruhe, Germany*

Received December 19, 2008. Revised Manuscript Received April 1, 2009

We show that fluorescence correlation spectroscopy (FCS) using a commercial spectrometer can be applied to passive microrheological (MR) experiments. The method probes the local rheological properties of materials on length scales of the focus dimension of the confocal microscope. For a feasibility study, we performed measurements on a high molecular weight poly(ethylene oxide)−water solution to allow direct comparison of the results to previous studies using diffusing wave spectroscopy, quasielastic light scattering, and particle tracking methods. We were able to detect mean-square center-of-mass displacements ranging from somewhat better than $\langle \triangle r^2(t) \rangle \approx 100$ nm^2 up to above $\langle \Delta r^2(t) \rangle \approx 10^6$ nm^2. Thus, we were able to derive the bulk rheological shear moduli covering more than five decades in frequency (from $\omega \leq 10^{-1}$ rad/s to $\omega \approx 10^4$ rad/s). The MR results are compared to results obtained from conventional rheological experiments on the same samples using a rotational rheometer as well as a piezo-driven squeeze flow apparatus. Good agreement between MR results probing the local rheological properties and those obtained by the conventional methods measuring the macroscopic mechanical response is found in the whole frequency range. Spatial resolution in combination with the possibility of using small tracer beads open the opportunity to probe the local, length scale-dependent rheological properties in heterogeneous samples. Small tracer concentrations and small sample sizes make FCS spectroscopy a powerful tool in particular for biological and medical applications.

Introduction

In a conventional rheological experiment, the deformation of a sample in response to an externally applied stress or vice versa is measured in order to obtain information about the mechanical properties of materials and the underlying microscopic relaxation processes over a large time or equivalent frequency range.[1] These methods yield information about the bulk response averaged over the whole sample.

Microrheological (MR) experiments use probe particles of typically micrometer sizes to locally deform the sample.[2,3] Thus, MR gives access to the length scale-dependent changes of the mechanic response and dynamic processes in materials. It also allows the determination of the local mechanic response of heterogeneous samples. Because only small sample volumes of the order of microliters are needed, MR methods are in particular valuable whenever samples are difficult to obtain in large quantities as, for example, in many biological and medical applications.

Two classes of MR experiments can be distinguished. An overview over the different techniques is given in refs 2 and 3. The first class uses active manipulation of the probe particles by applying an external driving force. These techniques include, for example, the use of optical tweezers, electric and magnetic fields, and also atomic force microscopy. Active methods are useful if large stresses have to be applied to stiff materials as well as for investigations of nonlinear response and nonequilibrium phenomena. The second class of MR experiments exploits the Brownian motion of the tracer particles. Because no external forces are applied, passive experiments always operate in the linear viscoelastic regime. This class of MR experiments is in particular suitable for soft materials and includes, for example, video particle tracking, photo correlation spectroscopy with light, and X-rays. In case the size of the tracer particles is significantly larger than the structural dimensions in the material and if there is no specific interaction of the tracer particles with the components of the surrounding fluid, it has been shown that MR experiments measure the macroscopic mechanical response of the sample;[4,5] in case the tracer particle size becomes comparable to the internal structure, the MR experiments are sensitive to the local mechanical response effected by the microstructural environment in the vicinity of the probe particle.[6−8] Because of the small tracer particles, size inertia effects are small and become effective in the 1 MHz frequency range only. With light scattering techniques, frequencies up to 1 MHz were reached.[9,10] Typically, the frequency range covered by a MR experiment is much larger as compared to a single experiment using conventional rheometers. Details of the modulus and frequency range depend on the particulars of the different techniques used. For an overview, see, for example, Figure 1 of ref 2 and the discussion section in the Results and Discussion.

*To whom correspondence should be addressed. E-mail: s.rathgeber@mpip-mainz.mpg.de.

(1) Macosko, C. W. *Rheology, Principles, Measurements, and Applications*; Wiley-VCH: New York, 1994.
(2) Waigh, T. A. *Rep. Prog. Phys.* **2005**, *68*, 685–742.
(3) Gardel, M. L.; Valentine, M. T.; Weitz, D. A. In *Microscale Diagnostic Techniques*; Breuer, K., Ed.; Springer: New York, 2005.
(4) Mason, T. G.; Weitz, D. A. *Phys. Rev. Lett.* **1995**, *74*, 1250–1253.
(5) Mason, T. G.; Gang, H.; Weitz, D. A. *J. Mol. Struct.* **1996**, *383*, 81–90.
(6) Gardel, M. L.; Valentine, M. T.; Crocker, J. C.; Bausch, A. R.; Weitz, D. A. *Phys. Rev. Lett.* **2003**, *91*, 158302-1–158302-4.
(7) Wong, I. Y.; Gardel, M. L.; Reichmann, D. R.; Weeks, E. R.; Valentine, M. T.; Bausch, A. R.; Weitz, D. A. *Phys. Rev. Lett.* **2004**, *92*, 178101-1–178101-4.
(8) Liu, J.; Gardel, M. L.; Kroy, K.; Frey, E.; Hoffmann, B. D.; Crocker, J. C.; Bausch, A. R.; Weitz, D. A. *Phys. Rev. Lett.* **2006**, *96*, 118104-1–118104-4.
(9) Willenbacher, N.; Oelschlaeger, C.; Schopferer, M.; Fischer, P.; Cardinaux, F.; Scheffold, F. *Phys. Rev. Lett.* **2007**, *99*, 068302-1–068302-4.
(10) Oelschlaeger, C.; Schopferer, M.; Scheffold, F.; Willenbacher, N. *Langmuir* **2009**, *25*, 716–723.

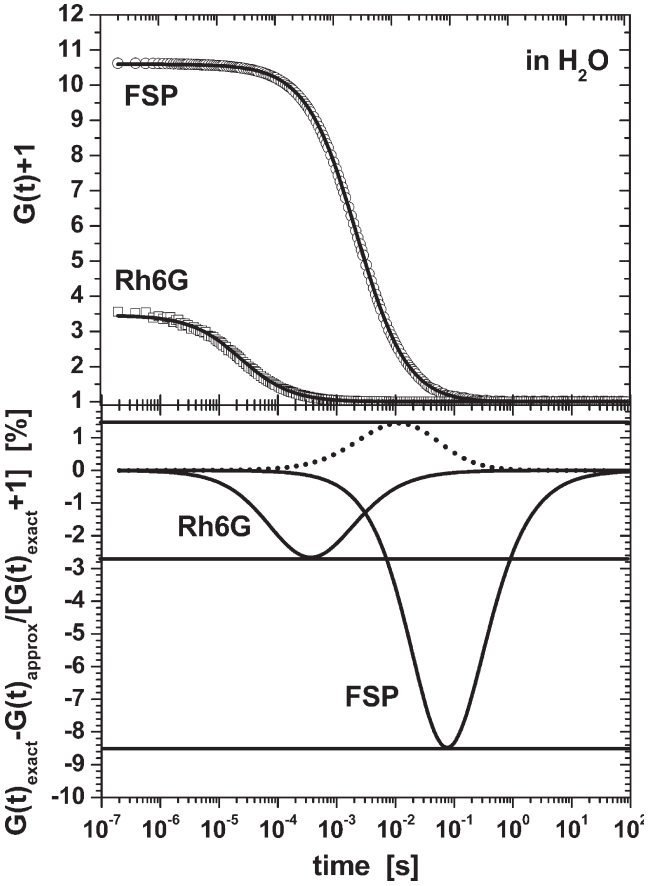

Figure 1. Correlation function $G(t) + 1$ measured with FCS for the FSP tracer beads and for Rh6G in water (markers). The solid lines show the fit results obtained by application of eq 5. In the bottom, the deviations between the exact (eq 5) and approximate solutions (eq 6) are shown (solid lines). For the FSP tracer beads, the deviation between the exact correlation function for finite-sized particles and results obtained from eq 5 with renormalized parameters $w_{xy}'^2$, $w_z'^2$, and $\overline{N}'$ is included (dotted line).

The aim of this publication is to prove for the first time the potential of fluorescence correlation spectroscopy (FCS) for MR measurements. FCS uses a confocal microscopy setup to monitor the spontaneous fluctuations of the fluorescence signal originating from the random motion of fluorescently labeled particles inside a defined submicrometer observation volume (~1 fL) irradiated by a focused laser beam.[11,12] The fluctuations can be quantified in their strength and duration by temporally correlating the recorded intensity signal. Often, the evaluation of FCS data is limited to the determination of local concentrations, mobility coefficients, or characteristic rate constants of inter- or intramolecular reactions, for example, by using two-color FCS. However, in case the FCS signal is due to concentration fluctuations of the labeled species, FCS measures the full self-correlation function (SCF) of the dynamics of the labeled part. Thus, not only effective diffusion or relaxation times but rather the mean-square center-of-mass displacement (MSD) as a function of time can be derived, allowing more detailed conclusions about the nature of the dynamics. Only few recent studies take advantage of this potential of FCS. This includes, for example, the work of Krichevsky and co-workers on the segmental dynamic of actin filaments[13] and superhelical DNA.[14]

Here, we would like to exploit the fact that FCS measures the full SCF from which the MSD can be derived to perform MR measurements. We see the advantage of FCS over other passive MR methods in the fact that FCS is capable of probing the local, rheological properties of heterogeneous samples on length scales of the focus dimension. In contrast to tracking methods in FCS, MR small tracer beads (diameters of 20 nm are commercially available) can be easily measured to determine the length scale-dependent rheological response. MR light scattering techniques like diffusing wave spectroscopy (DWS) and dynamic light scattering (single scattering DLS) are due to the large illumination volume not spatially resolved. Thus, in summary, due to spatial resolution in combination with the possibility of using small tracer beads FCS MR opens the opportunity to probe the local, length scale-dependent rheological properties in heterogeneous samples. Together with small tracer concentrations, small sample sizes and the fact that a commercial FCS spectrometer can be used, this makes FCS spectroscopy a powerful tool in particular for biological and medical applications, for example, for MR measurements on living cells.[15]

We use a commercial ConfoCor II Zeiss microscope (operated with ConfoCor III software) to measure the SCF over a time range from 10^{-7} s up to 1000 s. As a model system, we have chosen entangled poly(ethylene oxide) (PEO)−water solutions (M_w = 10^6 g/mol) doped with commercially available carboxylate-modified fluorescent polystyrene spheres (diameter $D = 126 \pm 6$ nm). By changing the amount of PEO, 2.5 and 5.0 wt %, respectively, the degree of elasticity of the mechanical response of the sample has been varied. The particular system was selected to allow direct comparison of our results to previous studies using light scattering and particle tracking techniques.[16−19] From the measured correlation functions, the MSDs of the tracer particles is derived. The so obtained MSDs are then converted to the bulk rheological responses in terms of the shear moduli using the approximate expressions introduced by Mason and Weitz.[17,20] We were able to determine the rheological shear moduli in a frequency range covering more than five decades (from $\omega \leq 10^{-1}$ rad/s to $\omega \sim 10^4$ rad/s). The MR results are compared to results obtained from conventional rheological experiments on the same samples using rotational rheology as well as a piezo-driven squeeze flow apparatus. Both methods together also cover a similar frequency range. Good agreement between MR results probing the local rheological properties and those obtained by the conventional methods measuring the macroscopic mechanical response are obtained.

Experimental Section

Samples. *Carboxylate-Modified Poly(styrene) Tracer Particles*. FluoSpheres were purchased from Molecular Probes, Inc. The fluorescent particles (FSPs) have an absorption maximum at 540 nm, an emission maximum at 560 nm and specified diameters of 100 ± 6 nm. Note that the actual particle diameter $D = 126 \pm 6$ nm determined by DLS deviates from the specified value (see the DLS section). The FSPs are provided in distilled

(11) Rigler, R.; Elson, R. S. *Fluorescence Correlation Spectroscopy: Theory and Applications*; Springer: Berlin, 2001.
(12) Krichevsky, O.; Bonnet, G. *Rep. Prog. Phys.* **2002**, *65*, 251–297.
(13) Bernheim-Groswasser, A.; Shusterman, R.; Krichevsky, O. *J. Chem. Phys.* **2006**, *125*, 084903-1–084903-11.
(14) Shusterman, R.; Gavrinyov, T.; Krichevsky, O. *Phys. Rev. Lett.* **2008**, *100*, 098102-1–098102-4.
(15) Weihs, D.; Mason, T. G.; Teitell, M. A. *Biophys. J.* **2006**, *91*, 4296–4305.
(16) Mason, T. G.; Ganesan, K.; van Zanten, J. H.; Wirtz, D.; Kuo, S. C. *Phys. Rev. Lett.* **1997**, *79*, 3282–3285.
(17) Dasgupta, B. R.; Tee, S.-Y.; Crocker, J. C.; Frisken, B. J.; Weitz, D. A. *Phys. Rev. E* **2002**, *65*, 051505-1–051505-10.
(18) Lu, Q.; Solomon, M. J. *Phys. Rev. E* **2002**, *66*, 061504-1–061504-11.
(19) van Zanten, J. H.; Amin, S.; Abdala, A. A. *Macromolecules* **2004**, *37*, 3874–3880.
(20) Mason, T. G. *Rheol. Acta* **2000**, *39*, 371–378.

water with a particle concentration of 2 wt %/(3.6×10^{13} particles/mL = 60 nM) according to manufacturer information. For the FCS experiments, the tracer particle stock solution was further diluted by a factor of 1/250, which corresponds to a FSP concentration of 0.24 nM.

PEO. PEO with a molecular weight of $M_w = 10^6$ g/mol (purchased from Aldrich) was dissolved in the water−tracer particle solutions. Samples with two different polymer concentrations, 2.5 (=2.2 vol%) and 5.0 wt % (=4.4 vol%), were prepared by dilution from the stock solution with the highest polymer content. Concentrations in volume fraction were calculated from the densities of PEO $\rho_{PEO} = 1.13$ g/cm^3 and water $\rho_{H_2O} = 0.998$ g/cm^3 at 20 °C. The solutions were kept in an incubator for 10 days at 40 °C. Gentle shaking twice a day ensured complete dissolution of the polymer and homogenization of the solution.

The mesh size $\xi = R_g (c^*/c)^{0.75}$ (c is the polymer concentration) of the PEO solutions can be estimated using the following relations for the radius of gyration R_g and the overlap concentration c^*: $R_g = 0.0215\ M_w^{0.58 \pm 0.03}$ [nm] and $c^* = M_w/(4\pi/3 N_A{}^3)$, where M_w denotes the PEO molecular weight and N_A is Avogadro's constant.[21,22] For the 2.5 and 5.0% PEO−water solution, being well above the overlap concentration $c^* = 0.15$ wt % (=0.13 vol%), the mesh sizes 7.9 and 4.7 nm are obtained, respectively. The tracer particles are significantly larger, 16 and 27 times, respectively, than the mesh size in the two PEO solutions. Thus, in the experiment, the bulk rheological response rather than the local rheological response should be measured.

DLS. The diffusion coefficients of the tracer particles were determined by an independent measurement by means of DLS using a homemade apparatus equipped with a near-infrared diode laser. The laser provides vertically polarized light at a wavelength of 831.5 nm with a power output of 80 mW (maximum of 60 mW on the sample). The crucial point is that this laser wavelength lies far outside of the absorption bands of the tracer particles. To avoid detector artifacts, the pseudo cross-correlation function was calculated by a hardware correlator, correlating the intensities detected by two avalanche diodes (see Figure 1S in the Supporting Information). A lag time range from 0.2 ms up to 300 s was covered. DLS spectra were taken in 10° steps for scattering angles between $\theta = 30$ and 150°. Thus, a scattering vector range from $q = 0.5210 \times 10^{-3}$ to 1.944×10^{-3} nm^{-1} was covered. Using a circulating temperature bath, the temperature at the sample position was kept fixed to 293.2 ± 0.1 K. Samples with a solid concentration from 6.7×10^{-3} down to 4.6×10^{-4} wt % were measured. Samples were prepared by dilution from the stock solution of FluoSpheres (FSPs) provided by Molecular Probes, Inc. The water used for dilution was filtered beforehand. For more details on the experimental setup, see the Supporting Information.

The z-averaged diffusion coefficient $\langle D \rangle$, the average bead hydrodynamic radius $\langle R_h \rangle$, and the width of the distributions, ΔD and ΔR_h, respectively, as a measure the polydispersity of the FSPs were determined using two different approaches: (1) CONTIN analysis[23] and (2) cumulant method[24] (see Figure 1S in the Supporting Information). We obtained $\langle D \rangle = (3.4 \pm 0.2) \times 10^{-12}$ m^2/s and $\Delta D/\langle D \rangle = 9\%$ from which the hydrodynamic radius can be determined to be $\langle R_h \rangle = 63 \pm 3$ nm using the Stokes−Einstein relation. In the insert of Figure S1 of the Supporting Information, the R_h distribution obtained from the CONTIN analysis is shown for comparison. The result $\langle R_h \rangle = 64$ nm with a half width of half maximum of 11% corresponds well to the result obtained using the cumulant analysis. For more details on the data evaluation, see the Supporting Information.

FCS. The fluorescence intensity correlation function was measured with a commercial confocal system using an inverted Axiovert 200 microscope equipped with a Confocor 2 module (Carl Zeiss GmbH, Germany) and a 40× C-Apochromat water immersion objective having a numerical aperture of 1.2. To avoid evaporation of the solvent, the samples were measured in a well-sealed, steel sample container with a 0.17 mm cover glass at the bottom (modified Attofluor cell chamber with top and bottom sealing, Molecular Probes, Inc.). The measurements were performed at room temperature (20 °C). For the excitation, the 544 nm line of a 25 mW argon laser was used. The emitted fluorescence light was detected by single photon counting via a 50% beam splitter in two avalanche photodiodes with preceding band paths (540−580 nm). The intensity correlation function was determined by cross-correlating the signal originating from the same sample volume but detected in two detectors via a software correlator using a multiple τ algorithm.[25] In this way, the artificial contribution to the signal from detector afterpulsing can be suppressed. The dimensions of the detection efficiency profile (typically $w_{xy} = 217 \pm 6$ nm and $w_z = 1150 \pm 60$ nm perpendicular and parallel to the beam direction, respectively) were determined by measuring the same carboxylate-modified fluorescent poly(styrene) tracer particles (FSPs) in water as reference before each MR experiment. The diffusion coefficients $D = (3.4 \pm 0.2) \times 10^{-12}$ m^2/s of the FSP was determined by DLS experiment (see the DLS section and the Supporting Information). Results were cross-checked using a 1 nM Rhodamine 6G (Aldrich) water solution as reference for which the diffusion coefficient was determined to be $D = (3.8 \pm 0.2) \times 10^{-10}$ m^2/s. The value compares well to the values determined by Enderlein and co-workers with double focus FCS for Rh6G from different suppliers.[26] They obtained $D = (3.9 \pm 0.3) \times 10^{-10}$ m^2/s and $D = (4.14 \pm 0.05) \times 10^{-10}$ m^2/s at a temperature of $T = 25$ °C for Rh6G purchased from Aldrich and Invitrogen, respectively. These deviations were attributed to the lower purity of the Rh6G from Aldrich.

Rheology. *Squeeze Flow*. Oscillatory squeeze flow experiments were performed using a piezo-driven axial vibrator (PAV). General theory of squeeze flow is covered in standard textbooks of fluid mechanics.[27] The theory of the PAV as well as the mechanical and electronic setup are thoroughly discussed elsewhere.[28,29] The actor is a thin-walled quadratic copper tube with a thick stainless steel plate on top. Four piezoelectric actuators are attached to two opposite walls of the tube to exert the vibrations, and four additional piezoelectric sensors are fixed to the remaining sides to pick-up the response signal. Direct coupling of excitation and detection is avoided by four partial cuts of the tube parallel to the longitudinal axis. This lower part of the device is surrounded by a double-walled cylinder allowing for circulation of a thermostatting fluid, and the temperature is controlled with an accuracy of ±0.04 °C. The whole setup is covered by a thick metal lid, which is the upper boundary of the gap and provides a complete sealing for the apparatus. The instrument is operated by a lock-in amplifier. The applied voltage of the driving piezos is proportional to the axial force, and from the complex ratio of the dynamic displacement of the lower plate (amplitude ≈ 5 nm) with and without fluid, one can calculate the complex squeeze stiffness K^* of the fluid using an appropriate mechanical equivalent circuit and solving its equations of motion. To calculate K^* from the ratio of the output voltage and the phase difference recorded by the lock-in amplifier with and without fluid, the mechanical properties (spring constant mass, resonance frequency) of the

(21) Devanand, K.; Selser, J. C. *Macromolecules* **1991**, *24*, 5943–5947.
(22) Cooper, E. C.; Johnson, P.; Donald, A. M. *Polymer* **1991**, *32*, 2815–2822.
(23) (a) Provencher, S. W. *Comput. Phys. Commun.* **1982**, *27*, 213–227. (b) Provencher, S. W. *Comput. Phys. Commun.* **1982**, *27*, 229–242.
(24) Schärtl, W. *Light Scattering from Polymer Solutions and Nanoparticle Dispersions*; Springer: Berlin, 2007.
(25) Weisshart, K.; Jüngel, V.; Briddon, S. J. *Curr. Pharm. Biotechnol.* **2004**, *5*, 135–154.
(26) Müller, C. B.; Loman, A.; Pacheco, V.; Koberling, F.; Willbold, D.; Richtering, W.; Enderlein, J. *Eur. Phys. Lett.* **2008**, *83*, 46001-1–46001-5.
(27) Bird, R. B.; Armstrong, R. C.; Hassager, C. *Dynamics of Polymeric Liquids. Fluid Dynamics*; Wiley: New York, 1987; Vol. *1*.
(28) Crassous, J. J.; Regisser, R.; Ballauff, M.; Willenbacher, N. *J. Rheol.* **2005**, *49*, 851–863.
(29) Kirschenmann, L. K. Aufbau zweier piezoelektrischer Sonden (PRV/PAV) zur Messung der viskoelastischen Eigenschaften weicher Substanzen im Frequenzbereich 0.5 Hz - 2 kHz bzw. 0.5 Hz - 7 kHz., Ph.D. thesis, Universität Ulm, 2003.

instrument itself have to be determined as described in ref 29. Finally, K^* is related to the complex shear modulus G^* and compressibility k_c^* by:[29]

$$\frac{1}{K^*} = \frac{2d_{gap}^3}{3\pi R_{gap}^4}\left(\frac{1}{G^*} + \frac{3R_{gap}^2}{2d_{gap}^2}k_c^*\right) \quad (1)$$

where R_{gap} is the radius and d_{gap} is the height of the gap (here, $R_{gap} = 10$ mm). The determination of G^* strongly depends on the exact knowledge of d_{gap}, which is determined by calibration using Newtonian liquids with viscosities between 1 and 2000 mPas. Here, gap heights between 15 and 100 μm have been used. The required sample volume is of the order of 100 μL. The exact value depends on the height of the gap. To avoid artificial compressibility from entrapped air, samples have to be degassed carefully. In principle, the measured G^* values have to be corrected for the k_c^* contribution. For the solutions investigated here, G^* is typically below 1000 Pa, and the compressibility is approximately that of water ($k_{c,w} = 4.6 \times 10^{-10}$ Pa^{-1} at 20 °C). Therefore, the compressibility correction of G^* is well below 5% and thus can be neglected. Dynamic shear moduli G^* in the range from 0.1 Pa to 10 kPa are accessible.

Rotational Rheometry. A rotational rheometer Thermo MARS II equipped with a cone−plate measuring cell (diameter $d_{CP} = 50$ mm, cone angle $\alpha_{cone} = 1°$) was used to perform small amplitude oscillatory shear experiments covering the frequency range from 0.01 to 100 rad s^{-1} at a strain amplitudes γ_0 between 0.5 and 2. Strain sweep experiments performed prior to the frequency sweeps confirm that this strain amplitude is sufficiently small to provide a linear material response at all investigated frequencies. A solvent trap was used to avoid evaporation of the solvent sample during the experiment.

Results and Discussion

In a confocal setup, the excitation laser light is directed by a dichroic mirror into a high-power objective, which focuses the light inside the sample. The fluorescence emission is collected through the same objective and is focused onto a pinhole, so that the laser beam waist inside the sample is imaged onto the pinhole aperture. The conjugation of the objective and the pinhole creates a spatial filter, which efficiently cuts the sampling volume to a diffraction-limited size. The detector records the intensity fluctuations of the fluorescent light. In our particular experiment, the intensity fluctuations result from fluctuations in tracer particle concentration c_T due to the fact that particles move out of and into the illuminated volume. To measure the pseudo cross-correlation, the fluorescent light is split by a 50% beam splitter into two equal beam paths and the correlation function $G(t)$ of the intensities measured by two independent detectors, I_1 and I_2, is calculated as

$$G(t) = \frac{\langle I_1(t')\, I_2(t+t')\rangle}{\langle I_1(t')\rangle\langle I_2(t')\rangle} \quad (2)$$

The intensity fluctuations I_i ($i = 1, 2$) can be converted into fluctuations in concentration c_T.

$$G(t) = \frac{\int\int \mathrm{PSF}(\vec{r})\,\mathrm{PSF}(\vec{r}')\,\langle \delta c_T(\vec{r}, t=0)\,\delta c_T(\vec{r}', t)\rangle\,\mathrm{d}\vec{r}\,\mathrm{d}\vec{r}'}{\left[\overline{c}_T \int \mathrm{PSF}(\vec{r})\,\mathrm{d}\vec{r}\right]^2} \quad (3)$$

where $\mathrm{PSF}(\vec{r})$ denotes the point spread function (detection efficienca profile) and $\overline{c}_T$ is the average tracer concentration. Assuming a Gaussian shape for $\mathrm{PSF}(\vec{r})$, the measured cross-correlation function can be directly related to the ensemble average of the MSD $\langle \Delta r^2(t)\rangle$ of the fluorescent tracer particles

$$G(t) = \frac{1}{V\overline{c}_T}\left(1 + \frac{2}{3w_{xy}^2}\langle \Delta r^2(t)\rangle\right)^{-1}\left(1 + \frac{2}{3w_z^2}\langle \Delta r^2(t)\rangle\right)^{-1/2} \quad (4)$$

Here, V denotes the illuminated volume and the product $V\overline{c}_T$ represents the average number of tracer particles $\overline{N}$ in the detection volume. w_{xy} and w_z measure the extension of the detection volume in the plane perpendicular and parallel to the beam direction, respectively. We want to point out that w_{xy} and w_z (commonly used in literature) are related to the full-width-of-half-maximum by $w_{FWHM,i} = [2\ln(2)]^{1/2} w_i \approx 1.18 w_i (i = xy, z)$. The focus dimensions have to be determined by measuring a substance with a known diffusion coefficient. In terms of the diffusion coefficient $D = \langle \Delta r^2(t)\rangle/(6t)$, one obtains

$$G(t) = \frac{1}{\overline{N}}\left(1 + \frac{4}{w_{xy}^2}Dt\right)^{-1}\left(1 + \frac{4}{w_z^2}Dt\right)^{-1/2} \quad (5)$$

Equation 4 can be solved analytically $\langle \Delta r^2(t)\rangle = fkt[G(t), \overline{N}, w_{xy}, w_z]$. In case $\langle \Delta r^2(t)\rangle \gg 3w_z^2/2 \approx 2 \times 10^6$ nm^2, the square-root term in eq 5 can be neglected and a simple relationship is found

$$\langle \Delta r^2(t)\rangle = \frac{3}{2}w_{xy}^2\left(\frac{1}{\overline{N}G(t)} - 1\right) \quad (6)$$

The accuracy of this approximation and its consequences for the reference measurements are discussed in the following. The average number of tracer particles $\overline{N}$ in the detection volume can be determined from the measured $G(t)$ data sets by extrapolation to $t = 0$ for each sample. For large entirely labeled particles, deviations from eqs 4−6 originating from finite size effects have to be considered.[30,31] They can be taken into account by replacing the point spread function $\mathrm{PSF}(\vec{r})$ in eq 3 by the convolution integral $\int \mathrm{PSF}(\vec{u} + \vec{r})\, f(\vec{r})\,\mathrm{d}\vec{u}$ where f describes the distribution of the fluorescent dye within the tracer particles. The integral is taken over the volume of the tracer particles. For the case $R \ll w_{xy} = 217$ nm, approximate expressions have been derived,[30,31] where w_{xy}^2, w_z^2, and $\overline{N}$ in eqs 4−6 are replaced by renormalized parameters w'^2_{xy}, w'^2_z, and $\overline{N}'$. The simple approximation given in ref 30 takes into account that the diffusion time of a finite-sized particle is increased as compared to an infinitively small particle by the time needed for the particles to travel a distance equal to its radius. This leads to the replacements $w'^2_{xy} = w_{xy}^2 + R^2$, $w'^2_z = w_z^2$, and $\overline{N}' = \overline{N}(1 + R_w^2)$ with $R_w = R/w_{xy}$. Because $w_z^2 \gg w_{xy}^2$, the effect on w_z is assumed to be negligible. Deviation from the exact solution for $G(t)$ of a homogeneously labeled tracer particle with $R = 63$ nm as used in our experiments are below 1.5% and are negligible within the accuracy of the MR experiment (see the dotted line in the bottom part of Figure 1). We want to point out that as long as the finite size effect can be taken into account by simple renormalization (which is not the case as soon as $R \approx w_{xy}$), it has no impact on the derivation of $\langle \Delta r^2(t)\rangle$ since w'^2_{xy}, w'^2_z, and $\overline{N}'$ are directly determined from the measured (reference) data obtained for the same tracer particles. Details are only important if one wants to derive the exact

(30) Starchev, K.; Zhang, J.; Buffle, J. *J. Colloid Interface Sci.* **1998**, *203*, 189–196.
(31) Wu, B.; Chen, Y.; Müller, J. D. *Biophys. J.* **2008**, *94*, 2800–2808.

dimension of the detection volume, for example, for the determination of tracer concentrations.

We determined the dynamic shear moduli for water solutions of high molecular weight PEO with different polymers contents, 2.5 and 5.0 wt %, respectively. The solutions show significant viscoelastic behavior. Fluorescently labeled PS colloids and Rhodamine 6G as a low molecular weight dye were measured as references.

Reference Measurements. The focus dimension was determined before each experiment by measuring fluorescent colloidal spheres [FluoSpheres (FSP), Molecular Probes, Inc.] in water as a standard with a known diffusion coefficient $D = (3.4 \pm 0.2) \times 10^{-12}$ m^2/s as determined by DLS (see above). For a cross-check, we also measured a water solution of a commonly used low molecular weight dye [1 nM, Rhodamine 6G (Rh6G)]. The corresponding FCS correlation functions are shown in Figure 1. The diffusion coefficient of the FPSs was determined with DLS using an infrared laser with a wavelength outside the absorption band of the FSPs (see the Experimental Section). By fitting eq 5 with finite size correction to the FCS correlation function of the FSPs, w_z and w_{xy} can be determined. Typical values vary around $w_{xy} = 217 \pm 6$ nm and $w_z = 1150 \pm 50$ nm. Errors are not only standard deviations obtained by a single fit of the intensity correlation function of the FPSs but rather take into account the error induced by the reference measurement relative to a standard. With the so determined cross-section dimensions, a fit of the FCS cross-correlation function of the Rh6G yields a diffusion coefficient of $D = (3.8 \pm 0.2) \times 10^{-10}$ m^2/s. The value compares well to the values determined by Enderlein and coworkers with double focus FCS for Rh6G from different suppliers.[26] A fit of the Rh6G data is not sensitive to the vertical focus dimension w_z. The reason becomes obvious if one compares the theoretical curves obtained from eq 5 with those calculated using the approximate expression given in eq 6. The deviation between the exact prediction and the approximation are rather small and are invisible in the presentation of the correlation function. They can be better visualized by plotting the difference between both solutions (see solid lines in bottom part of Figure 1). For the FSP tracer beads, the deviation between the exact correlation function for finite-sized, homogeneously labeled particles and results obtained from eq 5 using simple renormalization of the parameters w'^2_{xy}, w'^2_z, and $\overline{N}'$ is included (dotted line). Because $w^2_{xy}/w^2_z \ll 1$, the square root term in eq 5 becomes only effective in the tail of the correlation function when $\langle \Delta r^2(t) \rangle \approx 3w_z^2/2$. Deviations are still small but become significant for the FSPs. Because of the high dye density per particle, the correlation function of the fluorescent colloids can be measured with much higher accuracy at lower particle concentrations as compared to that of a low molecular weight dye. Hence, the fit to the correlation function of the FSPs is sensitive to w_z, whereas the fit to the correlation function of the Rh6G is not.

MSD. Figure 2 shows the FCS correlation functions of the FSPs in the PEO solutions. For better comparison, the amplitude of the correlation function $G(t = 0) = \overline{N}'^{-1}$ of the 5.0% PEO solution was slightly adjusted to match the one of the 2.5% PEO solution. Originally, $\overline{N}' = 0.100$ and 0.095 for the 2.5 and 5.0% PEO solutions, respectively. Figure 3 presents the MSDs of the FSPs in the PEO solutions and in pure water, which were derived by application of eq 4 (black markers) and its approximation (eq 6, red markers). For the limiting case of tracer particle diffusion in a purely viscous medium, $\langle \Delta r^2(t) \rangle \propto t$ holds; thus, the slope of the logarithmic time derivate is equal to one. In the opposite limit of pure elastic response of the matrix, the motion is completely arrested ($\langle \Delta r^2(t) \rangle$ = constant), and the slope of the logarithmic time derivate equals zero. Thus, in the general case of a viscoelastic medium, the logarithmic time derivate of the MSD lies between 0 and 1. The MSDs of the FSPs in pure water nicely

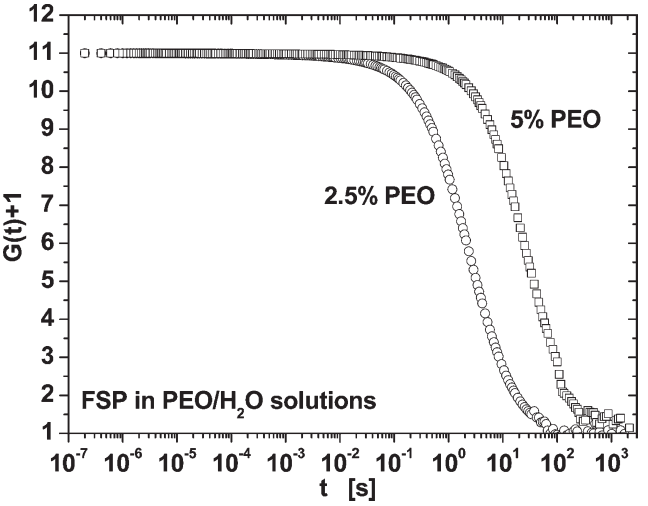

Figure 2. Correlation functions $G(t) + 1$ measured with FCS for the FSP tracer beads in PEO ($M_w = 10^6$ g/mol)−water solutions with different polymer contents; 2.5 and 5.0 wt %, respectively. For a better comparison, the amplitude [$G(t = 0) = \overline{N}'^{-1}$] of the 5.0 wt % data was slightly adjusted to match that of the 2.5 wt % data.

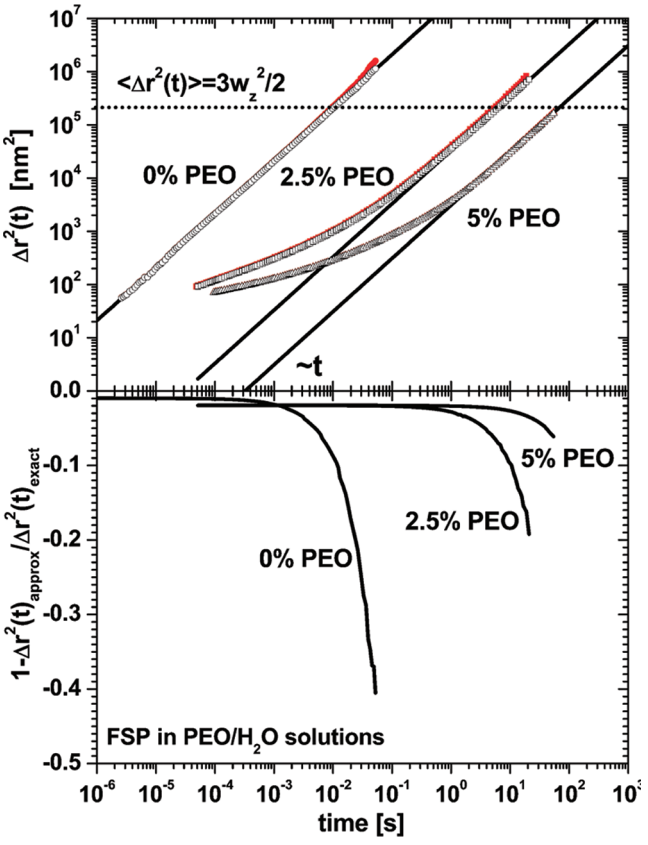

Figure 3. MSD of the FSP tracer beads (in pure water and in the PEO−water solutions) calculated from FSC correlation function using the exact (black markers) and approximate expressions (red markers) given in eqs 4 and 6, respectively (top), and the deviation between exact and approximate solution (bottom). The solid line shows the linear time dependence expected for free three-dimensional diffusion. The dashed horizontal line marks the condition $\langle \Delta r^2(t) \rangle = 3w_z^2/2 \approx 2 \times 10^6$ nm^2. For $\langle \Delta r^2(t) \rangle \ll 3w_z^2/2$, eq 6 is a good approximation.

follows the linear time dependence (marked by the solid lines), whereas the PEO solutions approach the ideal viscous behavior for long times only ($t \geq 1$ s). As expected for an entangled polymer solution, the latter exhibit significant viscoleastic response. For the FSPs in the PEO solutions, deviations between the exact and the approximate solutions of the MSDs lead to a small shift of the $\langle \Delta r^2(t) \rangle$ values of about 2% for times shorter than $t \cong 0.2$ s (see the bottom part of Figure 3). For longer times, when $\langle \Delta r^2(t) \rangle$ approaches the order of w_z^2, deviations become more significant. At the limit of the time window investigated here, deviations approach 20 and 6% for the 2.5 and 5 wt % PEO−water solution, respectively. However, this is still small on the logarithmic scale. Thus, eq 6 can be taken as a good approximation for the MSD over a wide range of time scales. Equation 6 also shows that as long as the focus can be described by a Gaussian shape, determination of the exact focus dimension is not a critical issue since an error in w_{xy} (here, $\Delta w_{xy}/w_{xy} \approx 2.5\%$) just leads to shift of the absolute values of the MSD with an error of $\Delta \langle \Delta r^2(t) \rangle / \langle \Delta r^2(t) \rangle = 2\Delta w_{xy}/w_{xy}$ (here, ≈5%).

Microrheology. Under the assumption that the local stress relaxation affecting the motion of the spherical tracer particles has the same spectrum as the bulk stress relaxation, one obtains a relation between the macroscopic viscoelastic shear modulus in the Laplace domain $\tilde{G}(s)$

$$\tilde{G}(s) = \frac{k_B T}{\pi R s \langle \Delta \tilde{r}^2(s) \rangle} - \frac{ms^2}{6\pi R} \tag{7}$$

Here, $\langle \Delta \tilde{r}^2(s) \rangle$ represents the ensemble averaged unilateral Laplace transform of the MSD: $\Delta \tilde{r}^2(s) = \int \exp(-st) \Delta r^2(t)\, \mathrm{d}t$, s is the Laplace frequency, R and m denote the tracer particle radius and mass, respectively, k_B is the Boltzmann constant, and T is the temperature. The first term originates from the thermal fluctuations dissipation of the matrix and represents the generalized Stokes−Einstein equation. The second term is due to inertia, which become effective at high frequencies but will be neglected here. Here, we look at the thermal motion of a tracer particle, that is, no driving forces are acting on the tracer particle. In this case, s can be substituted by the Fourier frequency $s = i\omega$ (no driving forces acting on the tracer particles), and an analogous relation is obtained in the Fourier domain.

$$G^*(\omega) = \frac{k_B T}{\pi R i\omega \langle \Delta r^{*2}(\omega) \rangle} \tag{8}$$

where ω is the experimentally accessible Fourier frequency and $\langle \Delta r^{*2}(\omega) \rangle$ represents the ensemble averaged Fourier transform of the MSD: $\langle \Delta r^{*2}(\omega) \rangle = \int \exp(-i\omega t)\, \Delta r^2(t)\, \mathrm{d}t$.

Numerical transformation of the experimental data sets may introduce errors in the shear moduli mainly caused by truncation errors. Therefore, Mason suggested an alternative evaluation procedure in which the MSD is expanded locally around the frequency $s = 1/t$ using a power law and retaining the leading term.[16,20] Weitz and co-workers later suggested the inclusion of the second-order logarithmic time derivate of the MSD.[17,32] The latter method can improve the results for the shear moduli in case the MSD is highly curved and the slope changes rapidly:

$$\langle \Delta r^2(t) \rangle \approx \langle \Delta r^2(t) \rangle \big|_{t=1/s} (st)^{\alpha(s)}\, (st)^{[\beta(s)/2]\ln(st)} \tag{9}$$

For example, the exponents $\alpha(s)$ and $\beta(s)$ are obtained from the first- and second-order logarithmic time derivate of the MSD, respectively,

$$\alpha(s) = \left. \frac{\partial \ln \langle \Delta r^2(t) \rangle}{\partial \ln t} \right|_{t=1/s} \tag{10}$$

$$\beta(s) = \left. \frac{\partial \ln \langle \Delta r^2(t) \rangle}{\partial^2 \ln t} \right|_{t=1/s} \tag{11}$$

Series expansion of $(st)^{[\beta(s)/2]\ln(st)} \approx 1 + [\beta(s)/2](st-1)^2 + \mathrm{O}[(st-1)^3]$ around $st = 1$ and Laplace transformation of eq 9 yields $s\langle \Delta r^2(s) \rangle \approx \langle \Delta r^2(t) \rangle|_{t=1/s} \{1 + [1 + \alpha(s) + \alpha^2(s)]\beta(s)/2\} \times \Gamma[1 + \alpha(s)]$, and together with eq 7, the shear modulus in the Laplace domain is obtained

$$\tilde{G}(s) = \frac{k_B T}{\pi R \langle \Delta r^2(t) \rangle|_{t=1/s}} \{1 + [1 + \alpha(s) + \alpha^2(s)]\beta(s)/2\}^{-1} \times \Gamma^{-1}[1 + \alpha(s)] \tag{12}$$

Here, Γ denotes the Γ function. Using $s = i\omega$, an analogous procedure leads to the complex shear modulus in the Fourier domain

$$G^*(\omega) = \frac{k_B T[\gamma - i\delta] i^{\alpha}}{\pi R \langle \Delta r^2(t) \rangle|_{t=1/\omega}\, \Gamma[1 + \alpha(\omega)]\, \{\gamma^2 + \delta^2\}} \tag{13}$$

with $\gamma = 1 + \{1 - [\alpha(\omega) + 1][\alpha(\omega) + 2]\}\beta(\omega)/2$ and $\delta = [\alpha(\omega) + 1]\beta(\omega)$. The complex shear modulus $G^*(\omega) = G'(\omega) + iG''(\omega)$ can be decomposed into the storage modulus $G'(\omega)$ (real part) and a loss modulus $G''(\omega)$ (imaginary part)

$$|G^*(\omega)| = \frac{k_B T}{\pi R \langle \Delta r^2(t) \rangle|_{t=1/\omega}\, \Gamma[1 + \alpha(\omega)] \sqrt{\gamma^2 + \delta^2}} \tag{14}$$

$$G'(\omega) = \frac{|G^*(\omega)|}{\sqrt{\gamma^2 + \delta^2}} \left\{ \gamma \cos\left[\frac{\pi}{2}\alpha(\omega)\right] + \delta \sin\left[\frac{\pi}{2}\alpha(\omega)\right] \right\} \tag{15}$$

$$G''(\omega) = \frac{|G^*(\omega)|}{\sqrt{\gamma^2 + \delta^2}} \left\{ -\delta \cos\left[\frac{\pi}{2}\alpha(\omega)\right] + \gamma \sin\left[\frac{\pi}{2}\alpha(\omega)\right] \right\} \tag{16}$$

In case second-order corrections are negligible [$\beta(\omega) = 0$, i.e., $\delta = 0, \gamma = 1$], Mason's results are obtained (see eqs 10−12 of ref 20). The results of Weitz and co-workers given in eqs 5 and 6 of refs 17 and 32 are reproduced only under the assumption $\alpha(s) + \alpha^2(s) \ll 1$, which is not satisfied for materials with significant viscous response. In practice, $\alpha(s)$ and $\beta(s)$ are determined locally, by piecewise fitting of $\ln\langle \Delta r^2(t) \rangle$ as a function of $\ln t$ to a second-order polynomial function using a sliding Gaussian window. However, for the system investigated here, the second-order contribution turned out to be negligible; hence, their contribution is not further discussed in the following. In the following, eqs 14−16 are used with $\delta = 0$ and $\gamma = 1$.

(32) Dasgupta, B. R.; Weitz, D. A. *Phys. Rev. E* **2005**, *71*, 021504-1–021504-9.

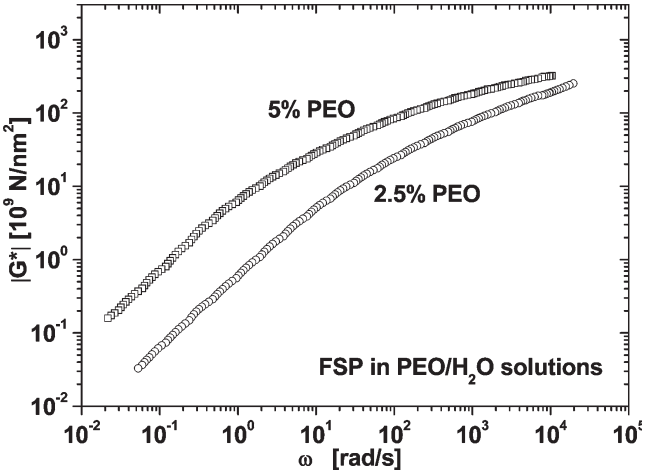

Figure 4. Norm of the complex shear moduli $|G^*(\omega)|$ obtained for the PEO−water solutions from the MSDs (see Figure 3) by piecewise fitting of $\ln\langle\Delta r^2(t)\rangle$ as a function of $\ln t$ to a linear function using a sliding Gaussian window and application of eq 14 with $\gamma = 1$ and $\delta = 0$.

In Figure 4, the norm of the complex shear modulus calculated by eq 14 is plotted as a function of the frequency. Because of the weak dependence of the Γ function $0.885 < \Gamma(x) \leq 1$ on arguments between $1 \leq x \leq 2$ $|G^*(\omega)|$ can be calculated with high accuracy over a large frequency range. The accuracy is determined by the error in the determination $\langle\Delta r^2(t)\rangle$ but is rather insensitive to the error-prone determination of the slope of $\langle\Delta r^2(t)\rangle$.

In Figure 5, the storage and loss moduli calculated by application of eqs 15 and 16 from the FCS data are compared to bulk rheological results obtained with a rotational rheometer and a piezo-driven squeeze flow apparatus on the same samples. The low frequency power law behavior expected for the storage ($\propto \omega^{-2}$) and loss modulus ($\propto \omega^{-1}$) of a viscoelastic fluid in the terminal flow regime are shown by the dashed lines. We obtain good agreement between the MR results and those obtained from conventional rheometry in terms of the frequency dependence of $G'(\omega)$ and $G''(\omega)$. We do not consider deviations between FCS and bulk rheological results observed in the low-frequency region of the 5.0 wt % PEO−water solution to be significant in particular, since the FCS reproduce the expected power-law behavior better than the bulk rheological data. However, to obtain an overlap in the absolute values the FCS data of the 5.0 wt % PEO−water solution have to be shifted by a factor of 2.5. For the data obtained for the 2.5 wt % PEO−water solution, no shift was necessary.

Possible causes for deviations between MR results and those obtained by conventional rheometry have been discussed in the literature to originate from a depletion layer around the tracer particle,[33,34] matrix−tracer interaction,[17,18] or due to tracer aggregation.[10] Furthermore, for small tracer beads, the MR experiment measures the local rheological response rather than the bulk rheological properties.[8] In the case of a locally heterogeneous sample, this can also occur on a longer length scale than the mesh size of the polymer solution.[18] We do not believe that tracer particle aggregation takes place in our samples. The tracer concentrations are small, and the measured average number of tracer particles in the illumination volume $\overline{N}$ is comparable for all solutions: (1) water solution ($\overline{N}' = 0.105$), (2) 2.5% PEO−water solution ($\overline{N}' = 0.100$), and (3) 5.0 wt % PEO−water solution ($\overline{N}' = 0.095$). Aggregation should lead to a significant decrease in $\overline{N}'$. The observed slight decrease is simply due to the fact that the polymer solutions were prepared by dilution of the PEO in the same FSP stock solution. Tracer bead−sample interaction should also have very little impact on the MR measurements. Lu and Solomon changed the surface chemistry of the tracer particles as well as their size.[18] For PEO−water solutions, only very little influence on the MR results was observed. The depletion layer, which is of the order of the mesh size, can be estimated to be 7.9 and 4.7 nm for the 2.5 and 5.0 wt % solutions, respectively (see the Samples section in the Experimental Section).[35] It can be considered to be too small to lead to significant changes in the rheological response and was also not observed in previous MR experiments on PEO−water solutions.[16−19] The experiment should measure the bulk rheological response rather than effects

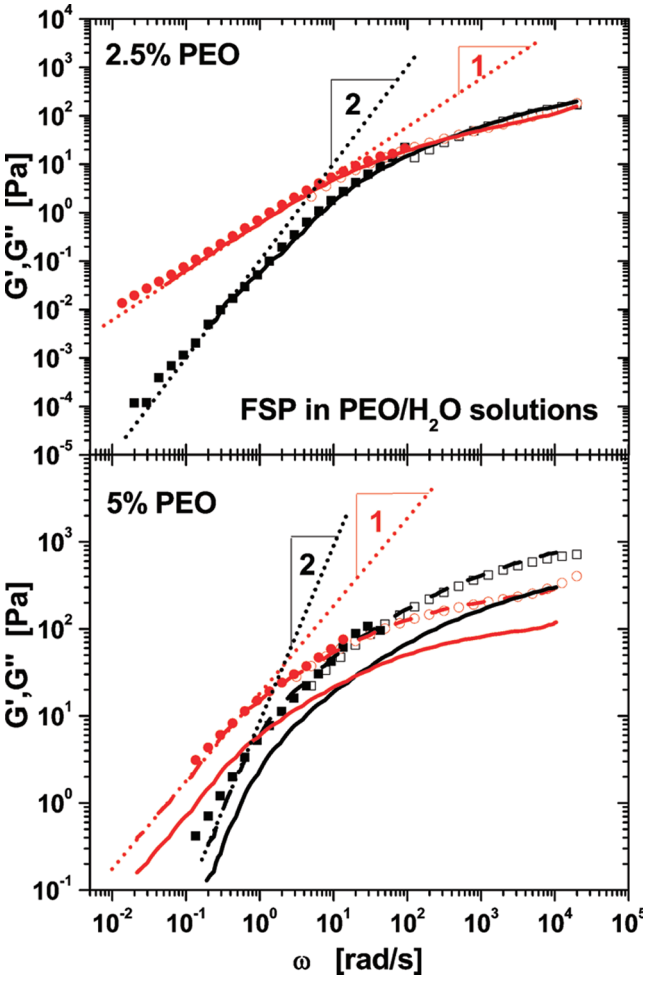

Figure 5. Storage (black, squares) and loss moduli (red, circles) of the 2.5 wt % (top) and 5.0 wt % (bottom) PEO−water solutions: Filled and open markers show the results obtained by bulk rheological methods using a rotational rheometer piezo-driven squeeze flow apparatus, respectively. The solid lines show the results obtained from the MR results derived from the MSDs by application of eq 14 to eq 16 with $\gamma = 1$ and $\delta = 0$. The dashed lines included for the 5.0 wt % PEO−water solution (bottom) show the MR results shifted by a factor 2.5 to match the absolute values of the bulk rheological data. The straight, dotted lines show the limiting low-frequency power-law dependence as expected for a viscoelastic fluid in the terminal flow regime.

(33) Chen, D. T.; Weeks, E. R.; Crocker, J. C.; Islam, M. E.; Verma, R.; Gruber, J.; Levine, A. J.; Lubensky, T. C.; Yodh, A. G. *Phys. Rev. Lett.* **2003**, *90*, 108301-1–108301-4.

(34) Huh, J. Y.; Furst, E. M. *Phys. Rev. E* **2006**, *74*, 031802-1–031802-10.

(35) Tuinier, R.; Lekkerkerker, H. N. W. *Macromolecules* **2002**, *35*, 3312–3313.

due to the local response because the tracer particles are significantly larger, 17 and 27 times, respectively, than the mesh size in the two PEO solutions. Furthermore, effects due to depletion and sensitivity to local response should become less effective with increasing concentration (decreasing mesh size) and should not only lead to a shift of the absolute values but rather change the frequency dependency of the moduli.[33,34] In summary, from the available data, no conclusions can be drawn about the origin of these deviations between bulk and mircorheological results. However, such shifts in absolute values have also been observed for DWS measurements on PEO−water solutions.[36] Therefore, we conclude that we obtain good agreement between MR results and those obtained by conventional rheology in terms of frequency dependency. The deviations in the absolute values are not yet understood, but they seem to be not an intrinsic problem of FCS microrheology.

The degree of accuracy of the calculation of the storage and loss modulus is strongly determined by the sensitivity of the sine and cosine term in eqs 15 and 16 on the slope of $\langle\Delta r^2(t)\rangle$. In the frequency range where the elastic character of the medium dominates ($\alpha \approx 0$), the cosine term changes only weakly as a function of α, whereas the sinus term is approximately a linear function of α. Thus, $G'(\omega)$ can be determined with the same accuracy as $|G^*(\omega)|$, whereas $G''(\omega)$ is strongly affected by errors in the determination of the slope of $\langle\Delta r^2(t)\rangle$. In a frequency range where the viscous character of the medium dominates ($\alpha \approx 1$), the situation is vice versa. This has in particular consequences for the low frequency region. In the tail of the FCS correlation function, uncertainties in the determination of the $G(t)$ and thus $\langle\Delta r^2(t)\rangle$ with $\alpha \approx 1$ are larger (longer time = smaller frequencies). This leads to larger uncertainties in the determination of $G'(\omega)$ and to a cutoff at higher frequencies as compared to the data obtained for $G''(\omega)$. However, we were able to determine the storage modulus in a frequency range covering about five decades ($\omega = 2 \times 10^{-1}$ to 1×10^4 rad/s). The loss modulus was determined in a frequency range covering almost six decades ($\omega = 2{-}5 \times 10^{-2}$ to 1×10^4 rad/s).

In the following, we would like to discuss the potential of FCS MR in comparison to other passive MR methods. From eqs 14 to 16 for the limiting case of an ideally elastic material with plateau moduli G_0 [$\alpha(\omega) = 0$], $G''(\omega) = 0$ and $G_0 = G'(\omega) = |G^*(\omega)| \propto [R\langle\Delta r^2(t)\rangle|_{t=1/\omega}]^{-1}$ can be derived. Thus, to probe samples with high plateau moduli, small tracer beads in combination with high spatial resolution in terms of detectable MSDs are necessary. For an ideally viscous sample with viscosity η [$\alpha(\omega) = 1$], $G'(\omega) = 0$ and $\eta = G''(\omega)/\omega = |G^*(\omega)|/\omega \propto [\omega R\langle\Delta r^2(t)\rangle|_{t=1/\omega}]^{-1}$ hold. For measurements on rather viscous samples, in addition, the low frequency limit has to be considered. For a viscoelastic fluid, one has to keep in mind that $\omega \leq 1/\tau$ ($\tau \approx \eta/G_0$ = relaxation time of the system) must be fulfilled to enter the flow regime and $\omega \geq 1/\tau$ has to be satisfied to resolve the plateau region.

With FCS MR, we were able to detect MSDs ranging from somewhat better than $\langle\Delta r^2(t)\rangle \approx 100$ nm^2 up to above $\langle\Delta r^2(t)\rangle \approx 10^6$ nm^2. As a correlator-based technique, FCS can easily cover a frequency range of 10^{-3} rad/s $\leq \omega \leq 10^6$ rad/s. In terms of tracer particle sizes, FCS is not restricted in the lower limit as it is capable to measure the dynamics of low molecular weight dyes. However, one has to keep in mind that for small particles, the experiment might not measure the bulk properties rather than local rheological response of the sample. For large entirely labeled particles, deviations from eqs 4−6 due to finite size effects have to be taken into account. When radii become similar to the focus dimension $R \approx \omega_{xy} = 217$ nm, in addition, details of the dye distribution within the tracer particles play a role. In principle, finite size and particulars of the dye distribution can be taken into account. However, proof for larger particles is pending, but one can also circumvent these difficulties by using center-labeled tracer particles,

With CCD detector-based laser particle tracking (LPT) methods, spatial resolution in terms of detectable MSDs of about $\langle\Delta r^2(t)\rangle \approx 25{-}100$ nm^2 is commonly achieved but usually limited to frequencies below $\omega \approx 100$ rad/s.[37−39] To obtain a sufficient signal-to-noise ratio, typically tracer particles with radii between 250 nm and 1 μm are used. However, there are also studies with much smaller tracer particles ($R = 50$ nm).[40] More recently, higher frame rates were achieved, giving access to frequencies up to $\omega \approx 10^3{-}10^4$ rad/s.[8,41,42] Because of intensity reasons, these studies are restricted to larger tracer particles with radii of about $R = 500$ nm to 1 μm. With improved detection techniques for the determination of the particle displacements such as laser interferometry or laser deflection particle tracking, MSDs beyond the nanometer level $\langle\Delta r^2(t)\rangle < 1$ nm^2 have been resolved. Because these methods probe a reduced sample volume only, they are not well-suited for studying long-time dynamics (frequencies below $\omega \approx 1$ rad/s).[43−45]

MR light scattering techniques like DWS and DLS (single scattering DLS) are due to the large illumination volume not spatially resolved. As correlator-based techniques, they cover the same frequency range as FCS. Tracer bead sizes that are typically varied between $R = 100$ nm and 1 μm are used.[17] The strength of DWS, a light scattering technique that exploits multiple scattering, originates from its capability to resolve small MSDs $\langle\Delta r^2(t)\rangle \approx 1$ nm^2 and short time scales in the microsecond range (frequencies up to MHz).[4,17,19] The drawback of this method is the high tracer concentration necessary to achieve multiple scattering. Furthermore, because of the fact that the maximal MSDs probed with DWS are well below 10^4 nm^2, this method is not suited to resolve the long-time dynamics.[4,17−19] In terms of the covered $\langle\Delta r^2(t)\rangle$ range, FCS MR should be comparable to single scattering DLS. However, in particular in single scattering DLS, constituents of the sample other than the tracer particles contributing to the scattering signal can cause severe limitations with respect to its application.

Conclusions

We have shown that FCS can be used for MR experiments. Experiments have been carried out using a commercial spectrometer. For a feasibility study, we have chosen high molecular weight PEO−water solutions as a model system. We were able to resolve MSDs of somewhat better than $\langle\Delta r^2(t)\rangle \approx 100$ nm^2 up to above $\langle\Delta r^2(t)\rangle \approx 10^6$ nm^2. Thus, we were able to derive the dynamic shear moduli over a frequency range covering more than five decades (from $\omega \leq 10^{-1}$ rad/s to $\omega \sim 10^4$ rad/s).

(36) Willenbacher, N.; Oelschlaeger, N. Private communication.

(37) Larson, T. H.; Furst, E. M. *Phys. Rev. Lett.* **2008**, *100*, 146001-1–146001-4.
(38) Xu, J.; Tseng, Y.; Carriere, C. J.; Wirtz, D. *Biomacromolecules* **2002**, *3*, 92–99.
(39) Raghu, A.; Somashekar, R.; Ananthamurthy, S. *J. Polym. Sci.: Part B* **2007**, *45*, 2555–2562.
(40) Tseng, Y.; Kole, T. P.; Lee, J. S. H.; Fedorov, E.; Almo, S. C.; Schafer, B. W.; Wirtz, D. *Biochem. Biophys. Res. Commun.* **2005**, *334*, 183–192.
(41) Papagiannopoulos, A.; Waigh, T. A.; Hardingham, T. E. *Faraday Discuss.* **2008**, *139*, 337–357.
(42) Caggioni, M.; Spicer, P. T.; Blair, D. L.; Lindberg, S. E.; Weitz, D. A. *J. Rheol.* **2007**, *51*, 851–865.
(43) Jonas, M.; Huang, H.; Kamm, R. D.; So, P. T. C. *Biophys. J.* **2008**, *95*, 895–909. Jonas, M.; Huang, H.; Kamm, R. D.; So, P. T. C. *Biophys. J.* **2008**, *94*, 1459–1469.
(44) Yamada, S.; Wirtz, D.; Kuo, S. C. *Biophys. J.* **2000**, *78*, 1736–1747.
(45) Buchanan, M; Atakhorrami, M.; Palierne, J. F.; MacKintosh, F. C.; Schmidt, C. F. *Phys. Rev. E* **2005**, *72*, 011504-1–011504-9.

FCS MR cannot compete with high resolution LPT methods or DWS in terms of spatial resolution of tracer particle displacements, but unlike FCS, these methods are not well-suited to cover the long-time dynamics. In terms of $\langle \Delta r^2(t) \rangle$ range, it is comparable to standard LPT methods and DLS (single scattering DLS). In contrast to standard LPT methods, high frequencies are easily accessed by FCS and the use of small tracer beads to probe the local, rheological response can be standard. As a fluorescence-based method, it is not sensitive to scattering contributions of other sample constituents as in particular single scattering DLS is. Together with the high doping concentrations needed for DWS measurements, this can impose severe limitations to the application of these light scattering techniques.

The spatial resolution in combination with the possibility of using small tracer beads for FCS MR opens the opportunity to probe the local, length scale-dependent rheological properties in heterogeneous samples. The spatial resolution of the FCS experiment is determined by vertical focus dimension ($w_z \approx 1\ \mu$m) or (if larger) by the maximal center-of-mass displacement measured $[\langle \Delta r^2(t) \rangle]^{1/2}$. Together with small tracer concentrations, small sample sizes, and the fact that a commercial FCS spectrometer can be used make FCS spectroscopy a powerful tool in particular for biological and medical applications, for example, for MR measurements on living cells.

Furthermore, we conclude with a comment on using a low molecular weight dye for the determination of the focus dimensions, w_{xy} and w_z, respectively. Because $w_{xy}^2/w_z^2 \ll 1$, a fit of the correlation function is only sensitive to w_z in the tail of the correlations function when $\langle \Delta r^2(t) \rangle \approx 3w_z^2/2$. A fit of the correlation function of a low molecular weight dye is normally not sensitive to w_z due to intensity limitations. Fluorescent colloids might provide an alternative approach. Because of the high dye density per particle, the correlation function of the fluorescent colloids can be measured with much higher accuracy at lower concentrations, which increases the signal amplitude. DLS experiments offer a simple access to an absolute determination of the diffusion coefficient of the colloids. However, one might also consider that for many applications the approximation given in eq 6 might be fully sufficient to describe the FCS correlation function.

Supporting Information Available: Details about the dynamics light scattering setup, correlation function measured for the FSP in water (Figure S1), and data evaluation (CONTIN and cumulant analysis) for the determination of their diffusion coefficient, hydrodynamic radius, and the width of the size distribution. This material is available free of charge via the Internet at http://pubs.acs.org.